University of Texas at El Paso
DigitalCommons@UTEP

Open Access Theses & Dissertations

2015-01-01

A Geophysical Study of the Castle Mountain Fault System and Matanuska-Susitna Valley Near Anchorage, Alaska

Shane Michael Schinagel
University of Texas at El Paso, smschinagel@gmail.com

Follow this and additional works at: https://digitalcommons.utep.edu/open_etd

 Part of the Geology Commons, and the Geophysics and Seismology Commons

Recommended Citation
Schinagel, Shane Michael, "A Geophysical Study of the Castle Mountain Fault System and Matanuska-Susitna Valley Near Anchorage, Alaska" (2015). *Open Access Theses & Dissertations*. 1154.
https://digitalcommons.utep.edu/open_etd/1154

This is brought to you for free and open access by DigitalCommons@UTEP. It has been accepted for inclusion in Open Access Theses & Dissertations by an authorized administrator of DigitalCommons@UTEP. For more information, please contact lweber@utep.edu.

A GEOPHYSICAL STUDY OF THE CASTLE MOUNTAN FAULT SYSTEM AND MATANUSKA-SUSITNA VALLEY NEAR ANCHORAGE, ALASKA

SHANE MICHAEL SCHINAGEL

Department of Geological Sciences

APPROVED:

Diane I. Doser, Ph.D., Chair

Laura F. Serpa, Ph.D.

Efrain J. Ferrer, Ph.D.

Charles Ambler, Ph.D.
Dean of the Graduate School

Copyright ©

by

Shane M. Schinagel

2015

Dedication

My graduate work is dedicated entirely to my wife, Chas, and our children, Austin, Ashlynn, Madilyn, and Cambrian.

To everyone who took the time to guide and direct me through challenging but rewarding life experiences: Chuck Schultz, Calvin Harris, Ed O., John Miller, MurrayVoight, Todd H., Joshua Villalobos, Diane Doser, Laura Serpa, Steve Appel, George Laguros, Ryan Stepler, and Laura Reich.

To my mother Joni Schinagel for a life-time of continued support.

A GEOPHYSICAL STUDY OF THE CASTLE MOUNTAIN FAULT SYSTEM AND MATANUSKA-SUSITNA VALLEY NEAR ANCHORAGE, ALASKA

by

SHANE MICHAEL SCHINAGEL, B.S

THESIS

Presented to the Faculty of the Graduate School of

The University of Texas at El Paso

in Partial Fulfillment

of the Requirements

for the Degree of

MASTER OF SCIENCE

Department of Geological Sciences

THE UNIVERSITY OF TEXAS AT EL PASO

May 2015

Acknowledgements

I would like to acknowledge Dr. Diane Doser for outstanding mentorship over the course of my undergraduate and graduate experience. Thank you to Felix Ziwu, Victor Avila, Manny Moncanda, and Niti Mankhemthong for help and technical support throughout this project. Thank you to Marathon Oil for funding my graduate education.

Abstract

The Castle Mountain Fault (CMF) is the closest (~50 km) active fault to Anchorage, Alaska. Located within the Matanuska and Susitna (Matsu) Valleys, the CMF shows repeated, unmistakable evidence for Holocene motion. Recent geologic studies estimate that this fault is capable of producing earthquakes of magnitude 7.0 – 7.1. The Anchorage metropolitan area (which includes the Matsu Valley) contains most of Alaska's population as well as vital shipping and transportation facilities that serve much of inland Alaska. Expected magnitude >7 earthquakes pose seismic hazards to the expanding Anchorage area.

While several mapping and trenching studies have been conducted along the CMF, geophysical investigations along the fault zone have been limited. We know very little about the subsurface structure of the fault and how it may control fault segmentation and depth of seismicity. The interaction between the CMF with adjacent, seismically active, reverse faults and folds is also poorly understood. A vital first step in predicting strong ground motion caused by events along the fault zone is to better understand the structure of the CMF. Using over 700 recently collected (between 2010 and 2011), closely spaced gravity observations, in addition to existing regional gravity, aeromagnetic, seismic reflection, well log data, and geologic information, we developed new 2D models of the deeper structure of the CMF system.

We created four 2D integrated forward models across the Castle Mountain Fault. These integrated models help to characterize differences between the western and eastern segments of the Castle Mountain Fault. Understanding structural changes across the CMF assists in determining how shallow and deep crustal controls impact seismicity of the CMF area. Our integrated models show a thick sequence of Tertiary to Mesozoic sediments overlying the Peninsular terrane basement at various depths within the area. We modeled several granitic intrusions that may have some effect on the mechanical behavior of the CMF where sediments are being pinched out and/or serpentinization is occurring.

Table of Contents

List of Tables

List of Figures

Introduction

The Castle Mountain Fault (CMF), located in south central interior Alaska <50 km north of downtown Anchorage, is a structural feature influenced by complex tectonic processes which actively deform the region (Figures 1 and 2). Geologic studies show that stress accumulation along the fault is capable of producing magnitude ~7 earthquakes (Haeussler et. al., 2002). As the Anchorage metropolitan area expands toward the Matanuska-Susitna (Matsu) Valley regions and closer to the CMF, potential seismic hazards increase significantly. Seismic hazards associated with elevated seismicity along the CMF motivate geophysical investigations aimed at better understanding the subsurface structure of the fault and how it may control local fault segmentation and depth of seismicity. Our 2D geophysical models of the deeper structure of the CMF system and Matsu Valley area (61-62°N Latitude and 148-152°W Longitude) will help to better understand the interaction between the CMF and other local faults and folds showing evidence for Quaternary motion. Understanding the relationship between the structure along the CMF and its influences on the faults seismic behavior is critical to better predicting strong ground motion from earthquakes occurring along the fault zone.

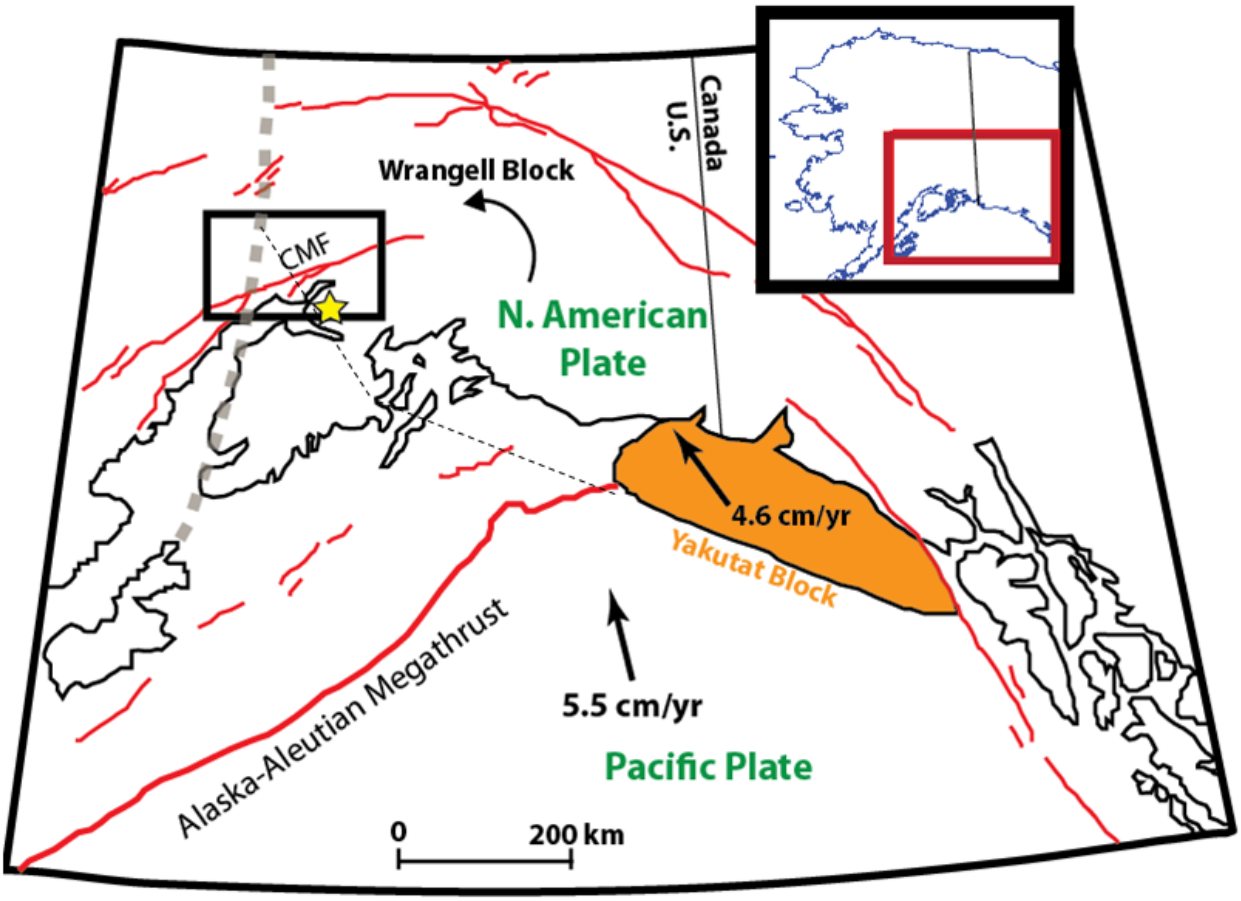

Figure 1. Tectonic setting of southern Alaska showing relationship between collision of the Pacific plate and Yakutat block with North American plate. Counter clockwise pointing arrow shows hypothesized direction of movement of the Wrangell block with respect to North America. Dashed gray line shows interpretation Wrangell block boundary. Thin dashed line represents southwestern edge of subducting Yakutat block. Black rectangle indicates study area and yellow star within study area is Anchorage. Bold red line is Alaska-Aleutian Megathrust and thin red lines are faults. Arrows show directions of plate motions relative to stable North America. Figure modified from Haeussler et.al, 2000.

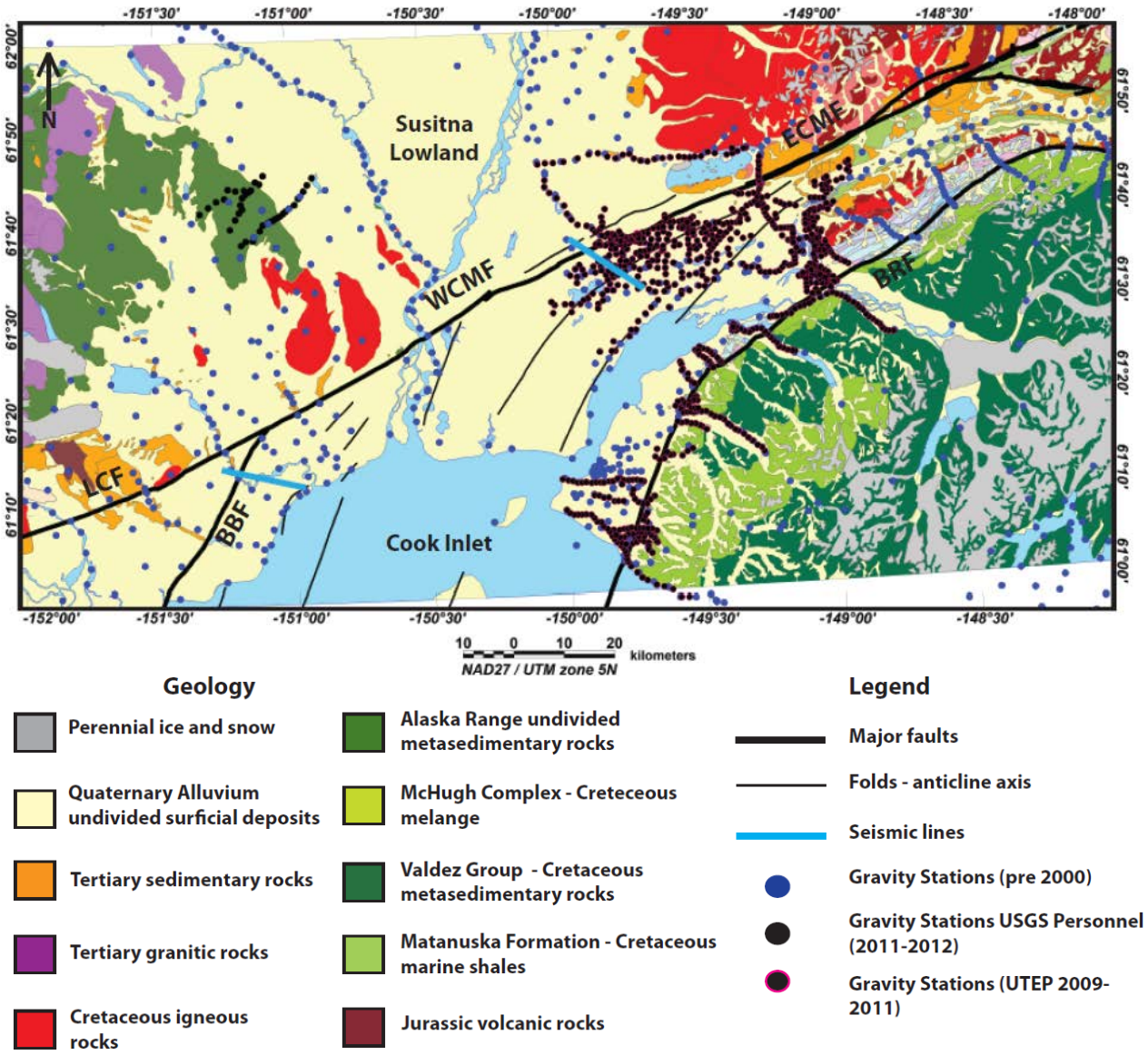

Figure 2. Geologic map of the Castle Mountain Fault and Matanuska-Susitna study area showing locations of all gravity measurements (simplified from Wilson et al., 2009). WCMF and ECMF are western and eastern Castle Mountain Fault. BRF is Border Ranges Fault, LCF is Lake Clark Fault, BBF is Bruin Bay Fault. NAD-North American Datum; UTM-Universal Transverse Mercator. Fault and fold data are digitized from Haeussler et al. (2000).

Background Geology

TECTONIC AND GEOLOGIC SETTING

Anchorage is Alaska's most populated city and is located in a zone of oblique subduction between the North American and Pacific Plates (Figure 1). Collision of the Yakutat microplate with North America complicates regional subduction resulting in a shallow dipping slab (approximately 3 degrees) beneath south central interior Alaska (Brocher et al., 1994). Regional folding and faulting occur in the upper crust as a result of oblique subduction in the Anchorage area. The most active (Neogene/Quaternary) crustal structures are concentrated between the Castle Mountain-Bruin Bay fault system and the Border Ranges fault (Figure 3) (e.g. Haeussler et al., 2000). Deformation studies along these structures suggest that 2 to 6% of cumulative North American/Pacific Plate convergence may be accommodated within the crust (Doser et al., 2004) through a combination of strike-slip and reverse faulting, and folding.

The Castle Mountain fault is located south and east of Quaternary volcanic centers and above the Aleutian megathrust convergent margin (Haeussler et al., 2014). The fault trends northeast within an active forearc basin system defining the southern margin of the Susitna basin and the northern margin of both the Cook Inlet Basin (CIB) and Matanuska Valley (Figure 3).
The Susitna Basin, recognized as an extension of the CIB, is a broad lowland with minimal outcrop exposure and subsurface data making it difficult to understand its stratigraphic and geologic history (Merritt, 1986). The CIB basin is bounded to the west by the Bruin Bay fault and to the east by the Border Ranges Fault System (BRFS) (Figures 2 and 3). The Matanuska Valley is composed mostly of middle Jurassic exhumed remnant portions of the forearc basin (Trop et al., 2005). The Alaska Range and Talkeetna Mountains, located northwest and northeast of the CMF represent mostly Late Cretaceous granitic arc rocks (Figure 2) while the Chugach Mountains to the southeast consist primarily of Permian to Eocene accretionary prism strata composed of two major lithotectonic assemblages: the older McHugh Complex mélange assemblage, and the younger metasedimentary rocks known as the Valdez Group. (Tysdal and Plafker, 1978; Pavlis and Roeske, 2007).

Extensive Quaternary glacial deposits cover most of the central-northern and southern portions of the CMF area. These undifferentiated glacial deposits unconformably overlie Late Eocene to Late Pliocene sedimentary rocks known as the Kenai Group observed within the CIB (Fig. 1; Hauessler and Saltus, 2011). Borehole date reveal that the Kenai Group contains cross-bedded to massive sandstones, siltstones, claystones, and shale with an estimated total thickness of ~2km near the basin axis (Plafker et al., 1989). Five nonmarine formations are classified within the Kenai group, including the Sterling, Beluga, Tyonek, Hemlock, and West Foreland Formations which overlie late Mesozoic sequences (Swenson, 1997). The late Mesozoic sequences are recognized as a succession of shallow-marine rocks of Early Jurassic-Cretaceous age with an approximate thickness of~8500m. These sedimentary deposits collectively define the forearc basin stratigraphic sequences that cover early Jurassic intrusive assemblages of the Peninsular terrane basement rocks.

The Border Ranges ultramafic assemblage (BRUMA), is identified among the Peninsular terrane basement rocks along the eastern CIB boundary (Debari and Coleman 1989; Plafker et al., 1989). The BRUMA primarily represents plutonic rocks ranging in composition from gabbro to tonalite with local ultramafic rock features (e.g., Burns, 1982; Plafker et al., 1994) and a fragmented crustal section of an Early Jurassic oceanic arc system (Plafker et al., 1989; Pavlis and Roeske, 2007).

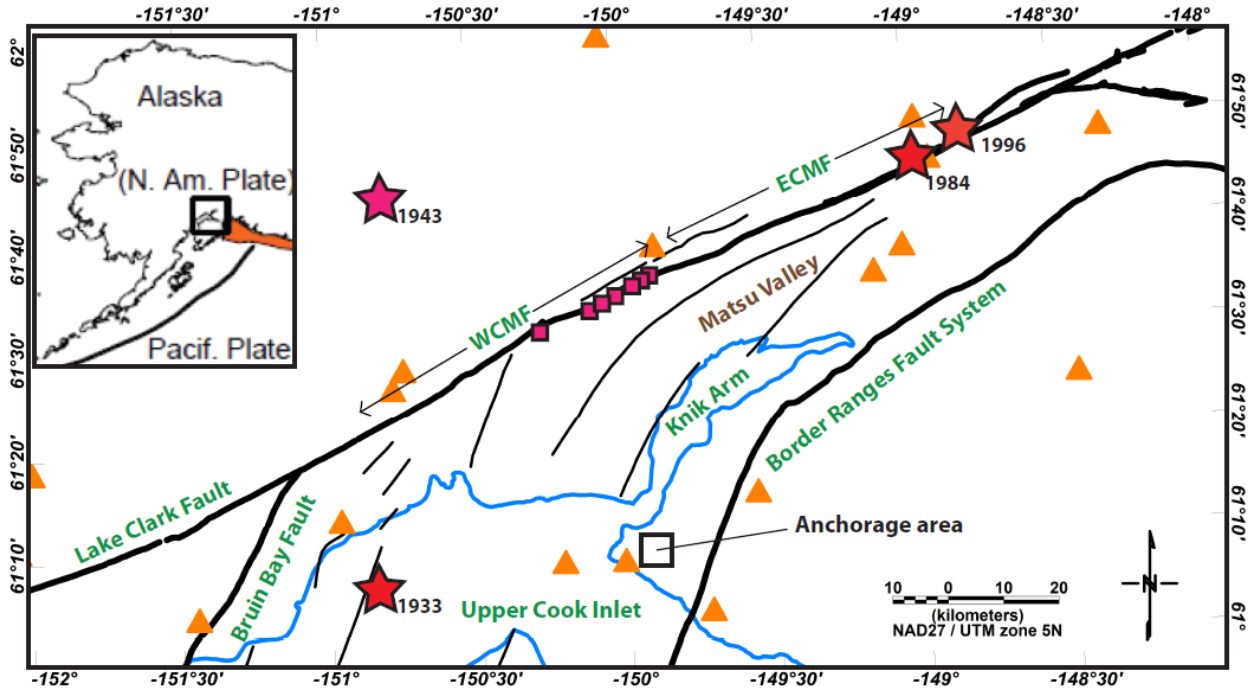

Figure 3. Map of study area showing major faults (bold black lines) and folds (thin black lines) from Haeussler et al. (2000) and Haeussler and Saltus (2011). Pink squares along WCMF are locations of previous trenching studies. Inset map at upper left shows location of study area in Alaska with respect to major tectonic plates and Yakutat microplate (offshore portion in orange). Bold black line in inset map is the Aleutian trench. Stars indicate important earthquakes discussed in text. Black open square is location of Anchorage. Orange triangles are seismograph stations.

Previous Studies

The Castle Mountain Fault is the only fault in the Anchorage region showing consistent evidence for repeated Holocene movement (Haeussler et al., 2000). Geological and seismological studies reveal that four significant earthquakes have occurred on the CMF over the past ~2700 years, and that the CMF remains capable of generating magnitude 6 to 7 earthquakes (Haeussler et al., 2000). The average recurrence interval for earthquakes along the CMF is estimated to be 700 years, with approximately 600 to 700 years having passed since the last high magnitude event occurred along this fault (Haeussler et al., 2000). Additional studies report fault slip rate estimates of 0.27 to 0.32 cm/yr along the western portion of the CMF (Willis et al., 2007). These estimates indicate that 1.6 to 2.2m of slip has built up along the fault since the last event (enough to generate a magnitude ~7 event). While the eastern portion of the CMF shows no evidence of Holocene faulting, moderate earthquakes have occurred along this part of the fault in 1984 (M_w =5.7) (Lahr et al., 1986) and in 1996 (M_L =4.6) (Figure 3). Paleoseismic data indicate that the timing of earthquakes along the western portion of the CMF is similar to that of events along the plate interface, suggesting a possible link between the megathrust and crustal faults located within the study area (Hauessler et al., 2002). Since the east and west strands of the fault have different current and past seismological behavior (east strand is presently more active while west strand has most recent surface offset), developing a new geophysical model of the CMF area is crucial to better understanding the structure along the fault and its seismological impact on the Anchorage region.

Previous geophysical studies along the CMF zone have been limited to analysis of a seismic reflection line crossing the eastern end of the western CMF (Figure 1), magnetic data, and regional borehole information. Seismic reflection data reveal long-wavelength open folds deforming early to middle Miocene strata southeast of the CMF's surface trace (Haeussler et al., 2000). This particular fault zone is a complex area of faulting and folding at least 3km wide which forms a flower structure (Haeussler et al., 2000).

A number of geologic studies have shown that the CMF displays a notable change in geomorphic expression along its trace. The western portion of the fault (Figure 3) displays linear, mostly south facing, and right-stepping scarps up to 2m high that cut late Quaternary glacial and fluvial deposits associated with the Susitna and Little Susitna Rivers for approximately 60 km. Numerous liquefaction features are located along the western CMF (Haeussler et al. 2002). In contrast, no evidence for Holocene faulting is detected along the eastern part of the CMF (Detterman et al., 1976; Hauessler, 1994) even though this portion of the fault is associated with recent seismicity (Lahr et al., 1986; Flores and Doser, 2005).

Adjacent to the CMF, the Upper Cook Inlet area contains the highest concentration of reverse faults and folds within the region. These structural features are likely a result of positioning above the southwestern edge of the subducting Yakutat microplate (Figure 6) that focuses transpressional deformation (Haeussler and Saltus, 2011).

Flores and Doser (2005) identified numerous shallow, seismically active features (likely faults or fault-cored folds) located close to Anchorage and the CMF. A subset of 4200 shallow earthquake relocations (<20km) occurring between 1964 and 1999 is shown in Figure 4a. More recent events, occurring between 2000 and 2014, were then taken from the Alaska Earthquake Information Center (AEIC) catalog and compared to those occurring between 1964 and 1999 (Figure 4b). By comparison, it is evident that prominent regions of seismicity observed between 1964 and 1999 continue to be active through 2000 – 2014.

Seismicity between the Upper Cook inlet and the western CMF is consistent with reverse motion along faults coring mapped folds, such as the Bell Island anticline (BI box, Figure 4a). Just north of the junction between the CMF and the Bruin Bay fault, a NNW striking band of seismicity is observed (Talachulitna region, TL, Figure 4a). Seismicity patterns along this fault

suggest a northeast dipping fault (Flores and Doser, 2005). Two focal mechanisms from the AEIC catalog occurring within this region are also consistent with eastward dipping reverse faulting.

Figure 5 shows a cross section of the seismicity along the eastern CMF (magenta NE trending rectangle, Figure 4a). Events occurring within 10 km of the fault were projected onto this cross section. The dashed rectangle on the cross section encloses aftershocks of the 1984 Sutton earthquake. The Sutton sequence corresponds to considerably deeper seismicity (15-20 km). Shallow events appear on both sides of the 1984 Sutton Sequence. Along-strike changes in earthquake depth may be controlled by variations in bedrock geology along the fault. The deeper seismicity near Sutton suggests that the seismogenic width of the CMF could be greater than that of other Alaskan crustal faults, such as the Denali (~12 km, Ratchkovski et al., 2003) fault. This newly suggested seismogenic width has important implications for estimating the maximum credible earthquake and strong ground motion expected from the CMF.

In 2010 and 2011 UTEP students collected over 700 gravity data points along numerous transects across the Border Ranges Fault System (BRFS) and the CMF (Figure 2). The work involved the development of a new gravity inversion approach for 3-D structures. The inversion method uses gridded surfaces bounding geologic units of varying density, where the gravity field is rapidly calculated using line elements (Cardenas and Ceberio, 2012). Initial 2.5-D and 3-D studies of the structure of the BRFS are illustrated in Mankhemthong et al. (2011) and Mankhemthong et al. (2012b, 2012c).

A simple Bouguer gravity anomaly map (Figure 6) based on available gravity data and seismicity relocated by Flores and Doser (2005) shows an increase in seismicity along the CMF associated with high gravitational anomalies north of the fault. The long wavelength

gravitational low, extending through Upper Cook Inlet and ending near the inferred southwestern edge of the Yakutat microplate (dashed white line, Figure 6), is interpreted as the extension of a mid-crustal serpentinite body previously imaged by Saltus et al. (2001) in middle Cook Inlet (Mankhemthong et al., 2011; Mankhemthong et al., 2012c). Mankhemthong et al., (2012c) modeled the gravitational low located east of Knik Arm as due to underplated sediment from subduction of the Yakutat microplate. Two cross sections showing an interpretation of these deeper, longer wavelength features using gravity and magnetic data are shown in Figure 8.

The relationship between aeromagnetic data from Saltus et al. (1999) and relocated seismicity (Flores and Doser, 2005) is shown in Figure 7. A strong magnetic high (>200nT) along the eastern edge of Upper Cook inlet is related to the highly magnetized rocks of the Border Ranges ultramafic and mafic assemblage (BRUMA). An extension of a mid-crustal serpentinite body modeled by Saltus et al. (2001) appears to be causing a moderate magnetic high (100nT-200nT) within Cook Inlet. Flores and Doser (2005) proposed a connection between the concentrated seismicity in Cook Inlet and the location of the serpentinite body. While much of seismicity associated with the CMF occurs in a magnetic low, seismicity in the Talachultina region is located within a magnetic high (Figure 7).

Preliminary 2.5-D models based on modeling of long wavelength signals in the regional gravity and magnetic fields are shown in Figure 8 (locations of cross section lines E-E' and F-F' are shown in Figure 7) (Mankhemthong et al., 2011; Mankhemthong et al., 2012c). These models will serve as a starting point for more detailed modeling of the crustal and upper mantle structure the CMF region (including Upper Cook Inlet and the Matsu Valley) within this study.

a) 1971-1999 (relocated)

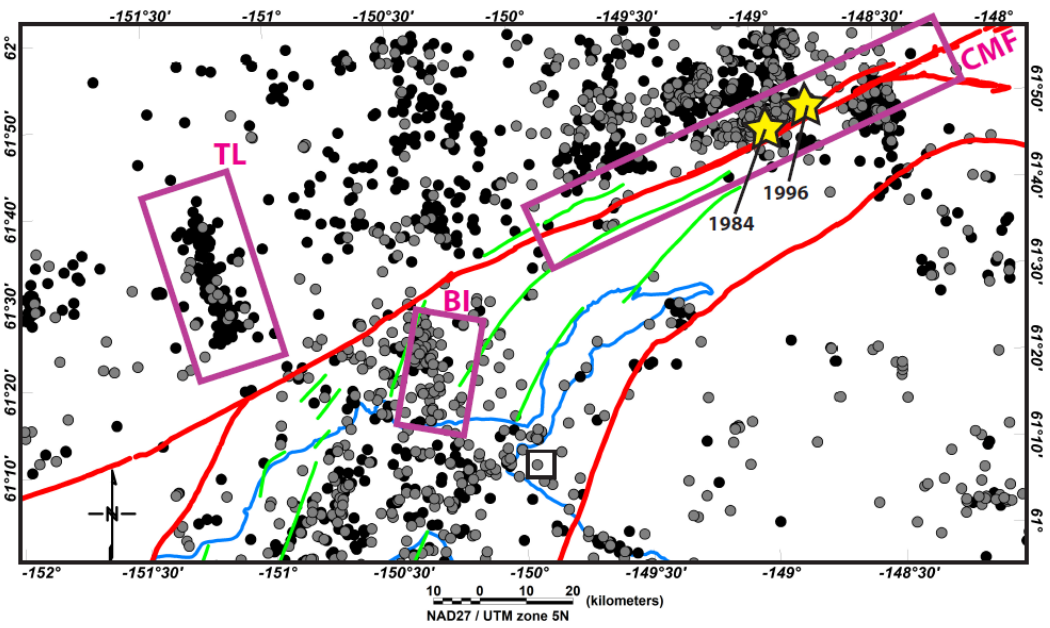

b) 2000-2014 AEIC catalog

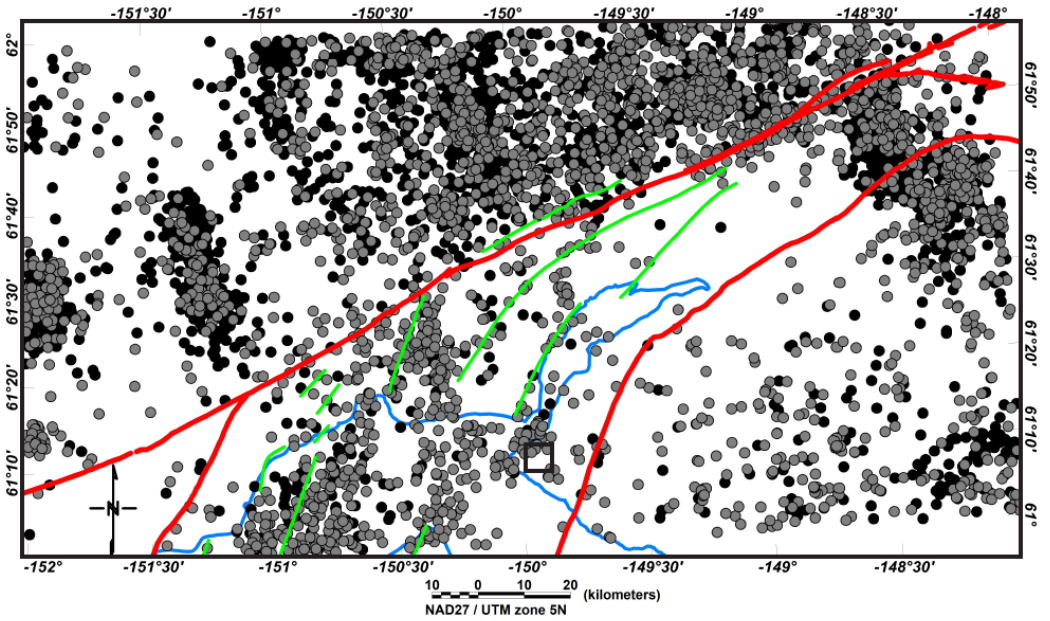

Figure 4. Seismicity of the study area. Black circles are events with depths <10 km and gray circles are events with depths of 10-20 km. All black and gray symbols are M<5 events. **a)** Magenta boxes indicate regions of intense seismicity related to the Castle Mountain fault (CMF), an unnamed fault in the Talachulitna region (TL) and Bell Island anticline (BI). The box labeled CMF is shown in cross section in Figure 5. Stars are the 1984 Sutton and 1996 eastern CMF earthquakes. **b)** AEIC catalog seismicity between 2000 and 2014.

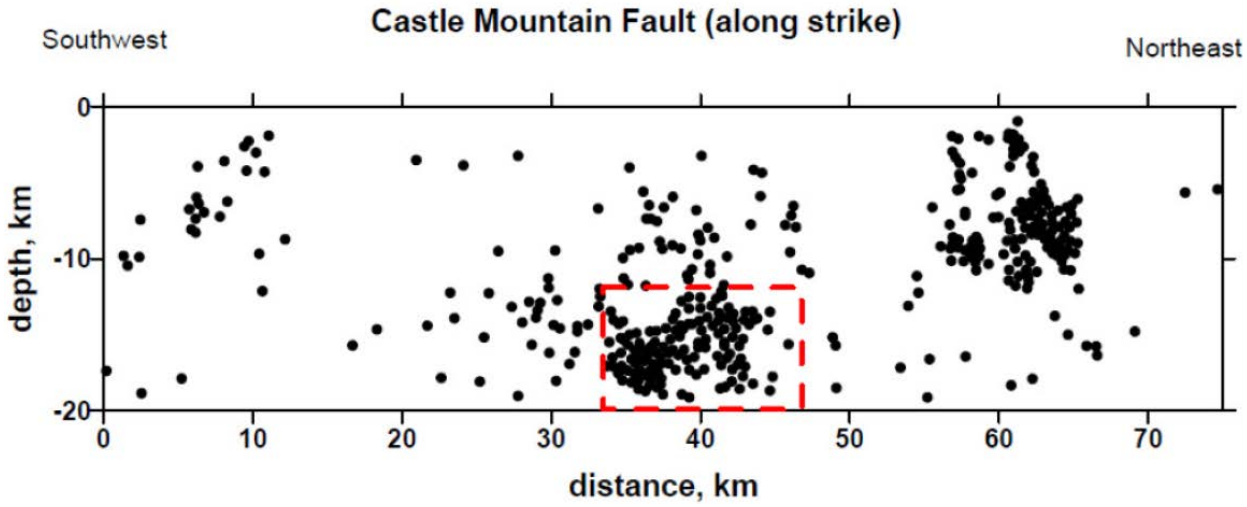

Figure 5. Cross section of seismicity along the Castle Mountain fault (see magenta rectangle in Figure 4a for location). Rectangle contains aftershocks of the 1984 Sutton Sequence.

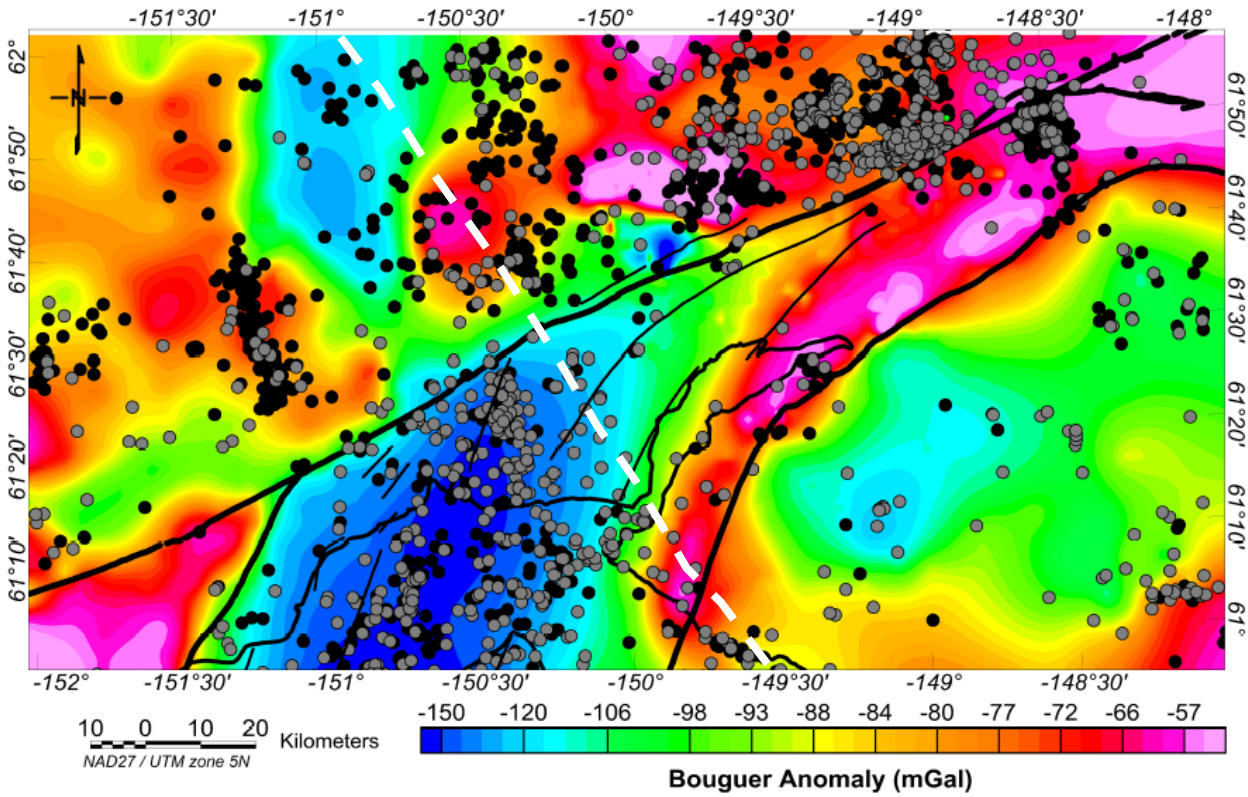

Figure 6. Bouguer gravity anomaly map of study area with relocated seismicity. Pink indicates zones of high gravitational anomalies while blue indicates zones of low gravitational anomalies. Dashed white line is the inferred southwestern edge of the Yakutat Microplate from Ebert-Phillips et al. (2006).

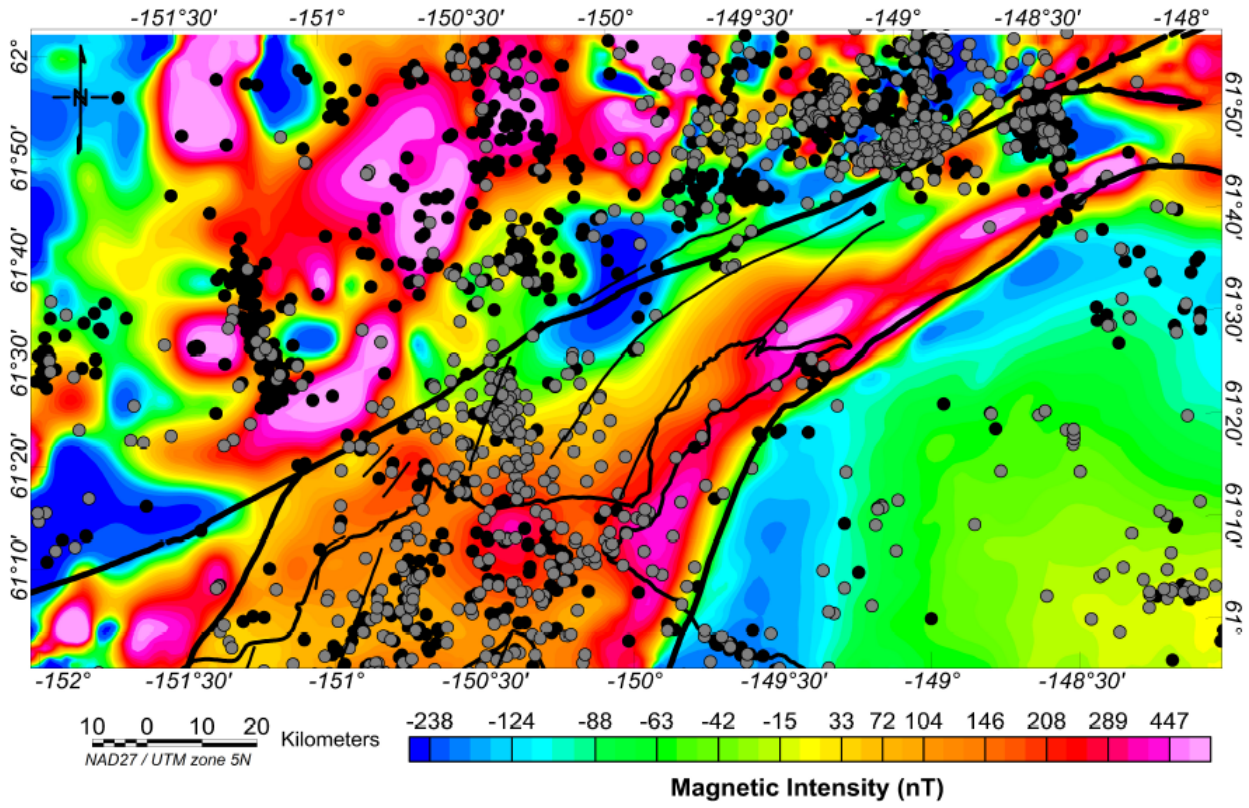

Figure 7. Aeromagnetic map of study area with relocated seismicity. Pink indicates zones of high magnetic intensity while blue indicates zones of low magnetic intensity. Aeromagnetic data from Saltus et al. (1999).

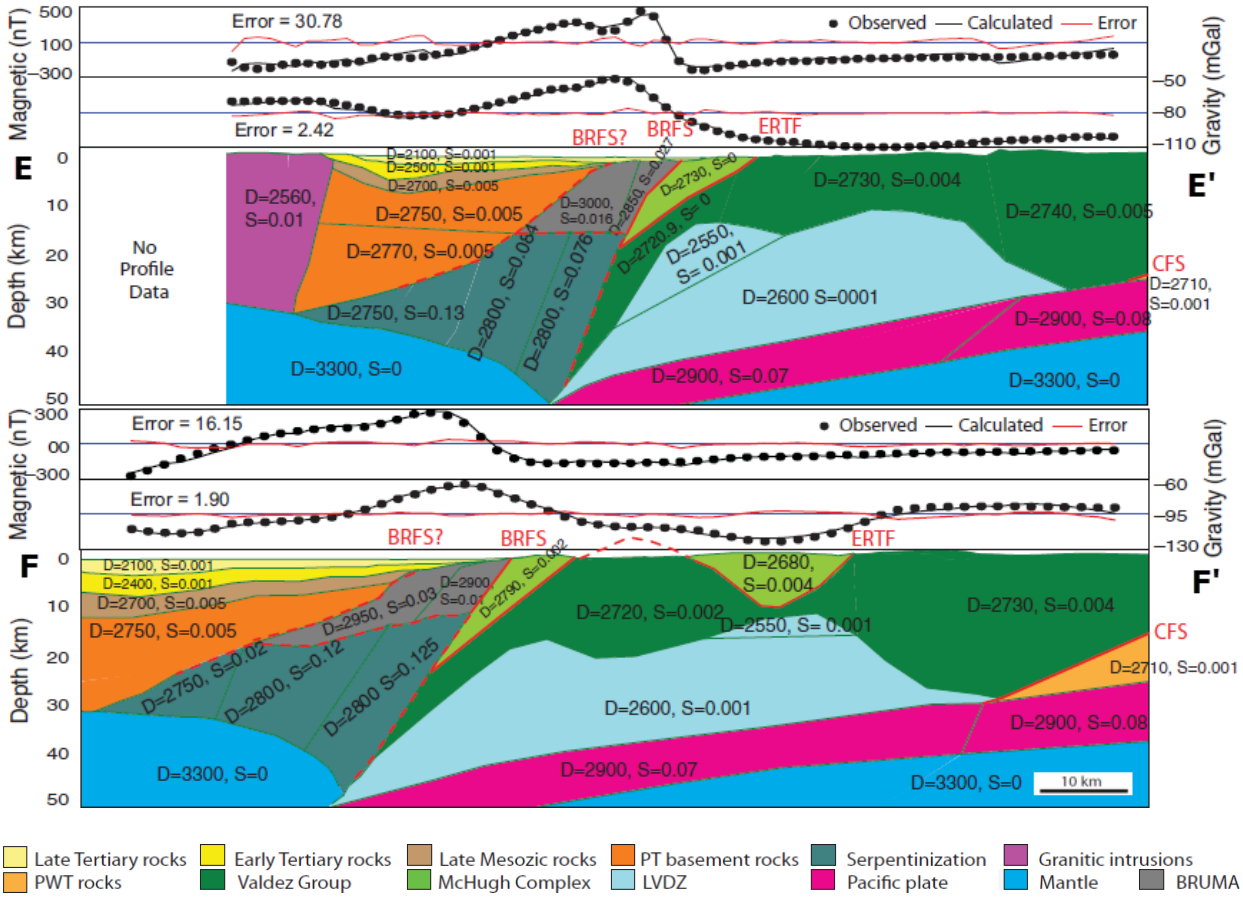

Figure 8. Structural models based on 2.5-D modeling of gravity and magnetic data for the study area (see location of cross sections in Figure 9). Solid red lines indicate known faults that extend to surface. The BRFS is the Border Ranges fault system; CMF is the Castle Mountain fault; ERTF is the Eagle River thrust fault. D is density and S is magnetic susceptibility. Profiles are vertically exaggerated by a factor of 0.4.

Methodology

GEOPHYSICAL DATA

Measured changes of the earth's gravitational field are a superposition of anomalies caused by density contrasts at various depths. These contrasts correspond to an apparent wavelength that is proportional to the depth of the lateral density changes. Geologic bodies close to the surface tend to produce shorter wavelengths with higher amplitudes, while deeper bodies relate to broad, longer wavelengths with smaller amplitudes. Observed changes in the gravity gradient can assist with geophysical interpretation of the subsurface structure of the area.

We used over 1600 gravity data points to map gravity changes caused by density contrasts across the study area (-148° to -152° longitude and 61° to 62° latitude) (Figure 9). About 700 of these data points were collected and processed between 2010-2011 by Mankhemthong et al. 2013. The 2010-2011 data were tied to established local absolute gravity stations and corrected to simple bouguer anomalies. A standard density of 2670 km/m^3 was applied for the Bouguer correction to remove the gravity slab effect (Burger et al., 2006). These data were combined with existing gravity data collected by USGS personnel over the western Susitna basin (black closed circles, Figure 9) during the summers of 2011and 2012 (R. Saltus, pers. commun., 2014) in addition to existing regional U.S. Geological Survey databases collected before 2000.

Similar to the gravity anomaly, the geometry of a magnetic anomaly depends on the shape of the causative body. However, magnetic anomalies also depend on the inclination and declination of the body's magnetization, the earth's local magnetic field, and the orientation of the body with respect to magnetic north. Variations in the magnetic field can often be used to determine locations of mineralization as well as regional structures within an area. Like gravity data, magnetic data can help constrain subsurface interpretation of geologic structures.

We utilized aeromagnetic data (compiled and reprocessed from Saltus and Simmons, 1997) to map magnetic intensities corresponding to the distribution of magnetic material and structural features within the study area (Figure 10). These data were extracted from four

separate surveys conducted between 1954 and 1977. Fight directions (north-south and east-west), altitudes (120-760 m), and flight line spacings (1600 m to 16,000 m), varied across surveys. By applying upward or downward continuation corrections and converting from level to drape as necessary, the original survey grids were adjusted to minimize differences at the boundaries resulting in a consistent survey specification of 305 m above ground (Saltus and Simmons, 1997). A reduction to pole filter was applied to the total intensity aeromagnetic data in order to eliminate lateral shift or distortion that might be caused if the magnetization and the ambient field are not both directed vertically (Blakely, 1995). Inclination and declination values of 73° and 25° are presumed values corresponding to the 1954-1977 time interval (Saltus and Simmons, 1997).

GRAVITY AND MAGNETIC ANOMALY MAPS

Reduced gravity and aeromagnetic anomaly maps were created using Geosoft Oasis Montaj software (Figures 9 and 10). Maps were gridded with the same 1000 m grid interval using a minimum curvature interpolation technique. Anomaly gradients were compared with known and inferred geologic features and relocated seismicity (Figures 4a and 4b).

We used fast Fourier transform Gaussian low (>20 km) and high (<20km) pass filtering analysis to enhance gravity and magnetic sources at different depths (Figures 11-13). Near surface bodies typically produce short wavelengths and larger amplitudes while deeper bodies produce broad, longer wavelengths of smaller amplitude. The filtering process helps delineate shallow from deep source locations, density contrasts, and zones of highly magnetized mineralization related to geologic features of interest.

GRAVITY ANOMALY INTERPRETATIONS

The most prominent features of the study area are the gravity lows related to the CIB, Susitna Lowland, and the Chugach Mountains, and the gravity highs associated with the BRUMA, Talkeetna Mountains, and various igneous plutons located north and southwest of the CMF (Figure 9).

The deepest gravity lows (-120 to -150 mGal) correspond well with the CIB boundaries and trend northeast along the basin axis. A northwestern oriented gravity low trends narrowly away from the western portion of the CMF broadening eastward toward the northern portion of the Susitna Lowland. The Susitna Lowland anomaly is bordered by gravity highs to the west and east. Gravity lows occurring within the Chugach Mountains are possibly related to underplated sediments linked to the southwestern edge of the subducted Yakutat microplate (Mankhemthong et al., 2013). The strongest gravity highs (>50 mGal) occur within the Talkeetna Mountains just north of the eastern portion of the CMF in a zone of dense metamorphic and igneous rocks. Gravity highs are also found in a belt along the eastern margin of the CIB trending sub-parallel to the BRFS. This belt likely represents subsurface high-density rocks of the BRUMA as modeled by Mankhemthong et al., 2013.

Strong gravity gradients occur at the northwestern edges of the CIB corresponding to the locations of the Bruin Bay and Castle Mountain faults (Figure 9) and are likely associated with volcanic arc material within the region. The CMF appears to be associated with 2 prominent gravity gradients between the CIB and Susitna Lowland, and between the western and eastern portions of the fault. These gradients appear to mark transitional zones from low density forearc basin deposits to high density igneous and metamorphic plutonic zones associated with the surrounding Talkeetna Mountains. The strong change from low gravity to high gravity from west to east along the CMF could also be related to the southwestern edge of the subducted Yakutat microplate.

High pass and low pass filter maps were created in order to emphasize both shallow and deeper structures within the area. However, only the low pass long-wavelength filter was used since sample site spacings were not sufficiently close enough together for analyzing the gravity signature of shallower features. Figure 11 shows the low pass Bouguer gravity anomaly map over the study area. The map has a wavelength cutoff of 20 km so all wavelengths shorter than 20 km were removed. Removal of the shorter wavelength features helps to determine the size and extent of deeper crustal bodies. The unfiltered map and the filtered map look very similar

suggesting that regional, deeper basement structures could be the major control on the surface expression of the gravitational signature of the study area.

MAGNETIC ANOMALY INTERPRETATIONS

The CMF area consists of a prominent northeast striking magnetic high related to the Cook Inlet basin forearc sedimentary deposits where gravity anomalies are lowest (Figure 10). The magnetic anomaly represents an abnormal feature for basin fill and is known as the Alaska Magnetic High. This zone could correlate with fluid serpentinization of altered lower forearc crust and/or mantle at 16-34 km depth (Saltus et al., 2001; Mankhemthong et al., 2013). Shallow sedimentary deposits within the basin (<15 km) are a less likely source of magnetic highs as the high pass (<20 km) filter map does not show such broadly distributed magnetic highs (Figure 12) as seen on the low pass filter map (Figure 13). Magnetic highs located to the west of the CIB and directly north of the lower western segment of the CMF are likely related to intrusive and extrusive bodies associated with the active volcanic arc (Saltus et al., 2001) occurring in areas with strong gravity highs (Figure 10) . The BRUMA magnetic high anomaly borders the eastern flank of the CIB sub-parallel to the BRFS in the Matanuska valley area and correlates well to strong gravity highs (Figure 10). This feature is observed in both the high pass and low pass filter maps (Figures 12 and 13) and is likely related to ultramafic bodies bordering the mountain front of the Chugach Mountains. Intense magnetic lows over the topographically high Chugach terrane suggest fewer and/or no magnetic source rocks within the accretionary complex (e.g., Saltus et al., 2007).

Strong magnetic highs occurring north of the western CMF likely correspond with both outcropping and buried plutons within the Susitna Lowland area (Figures 2 and 10). A strong magnetic gradient occurs across the western to eastern portions of the CMF and is visible on the unfiltered and Low pass filter maps. Low pass filtering analysis indicates long-wavelength magnetic lows suggesting deeper causative bodies along this part of the CMF. This feature occurs within the middle of the CMF and could be a deep structure transitional zone related to

the southwestern edge of the subducting Yakutat block (Figure 6). High pass filtering analysis shows short-wavelength magnetic highs occurring throughout zones of historic and recent seismicity along the eastern segment of the CMF (Figure 12). These anomalies correlate well with highly magnetized igneous and metamorphic zones located within the Talkeetna Mountains.

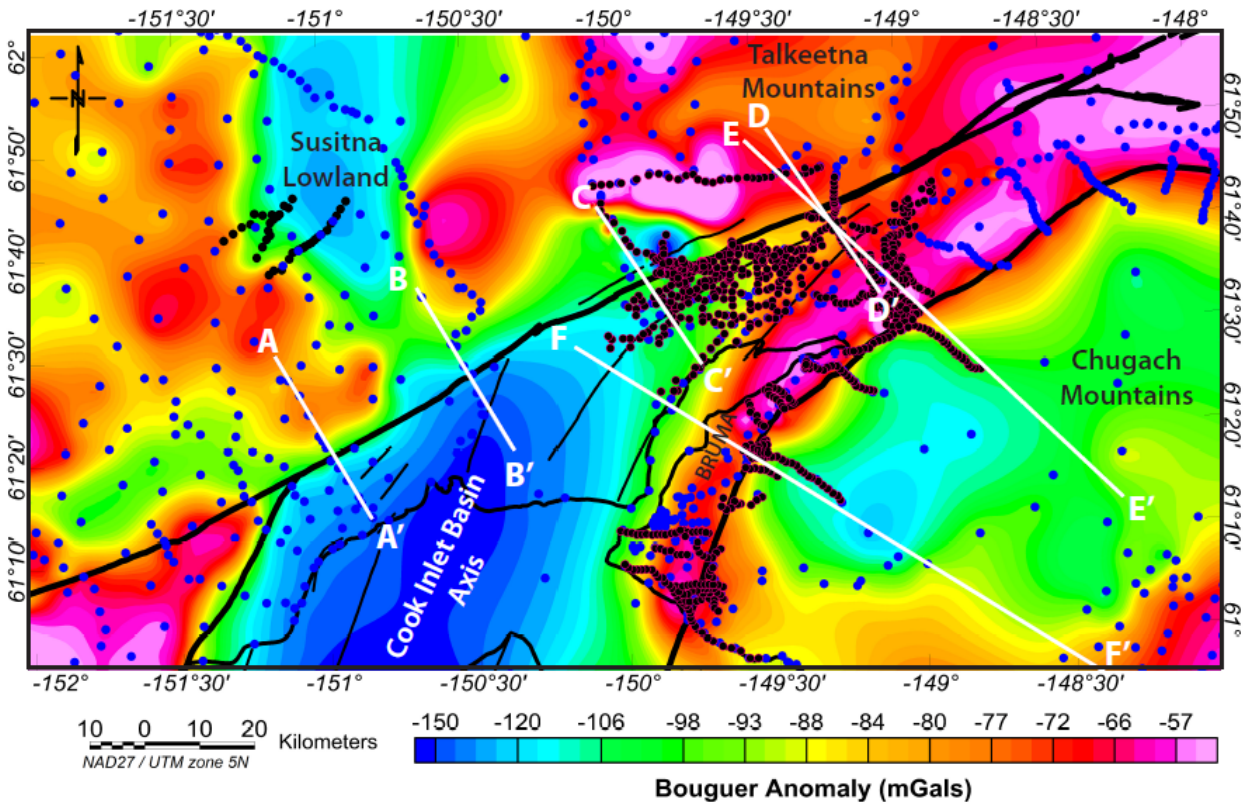

Figure 9. Bouguer anomaly map gridded at 1000 m. White lines A-A', B-B', C-C', and D-D' are locations of 2D integrated gravity and magnetic models analyzed in this study arranged from north to south along the Castle Mountain fault. Lines E-E' and F-F' are locations of existing 2D integrated gravity and magnetic models constructed by Mankhemthong et al., 2013. BRUMA is the Border Range ultramafic and mafic assemblages.

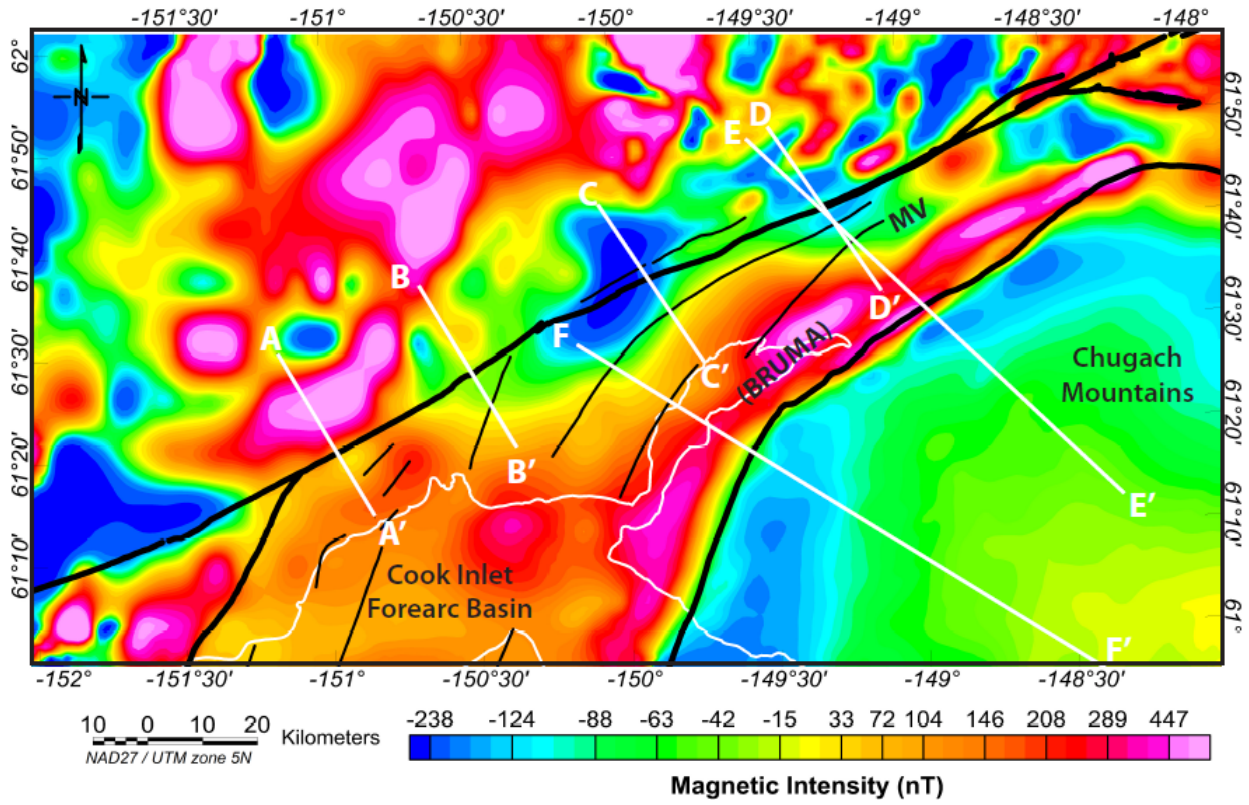

Figure 10. Total intensity aeromagnetic map gridded at 1000 m. White lines show location of 2D integrated gravity and magnetic profiles analyzed in this study. BRUMA - Border range ultra mafic and mafic assemblages. MV - Matanuska Valley.

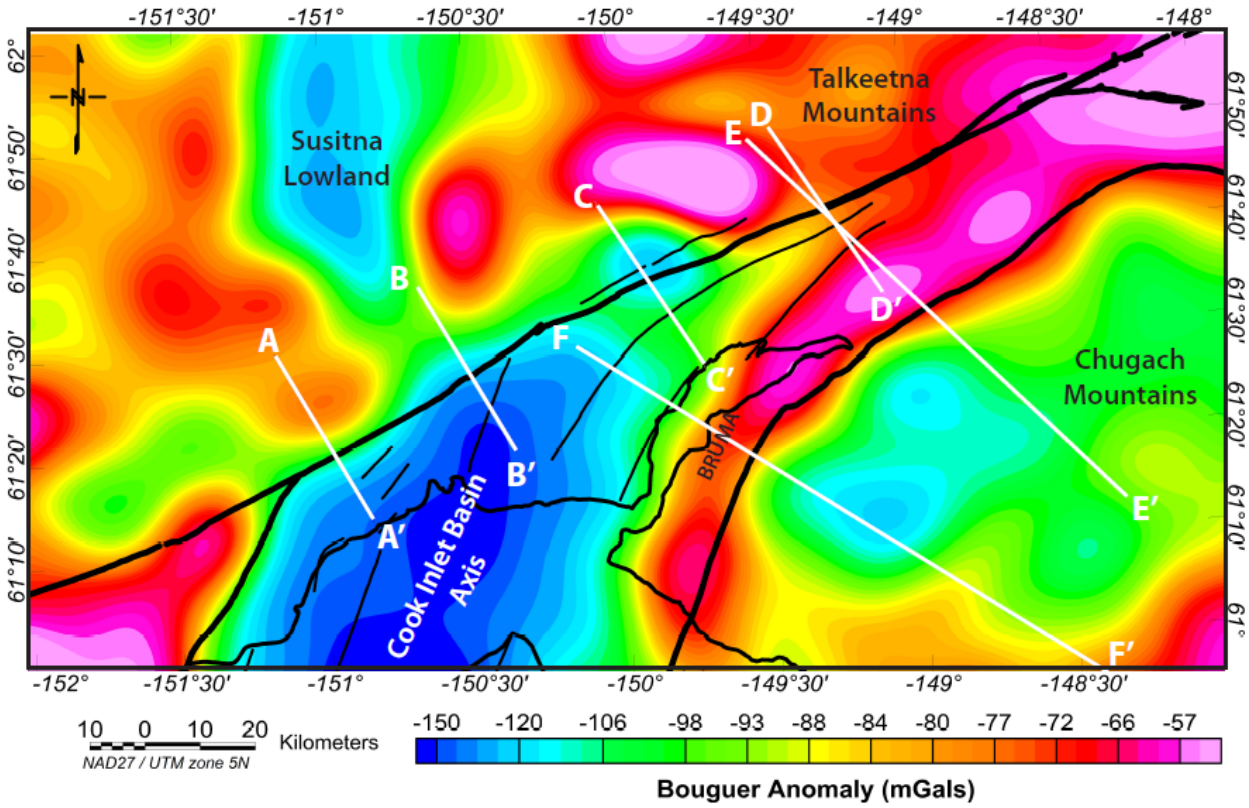

Figure 11. Long-wavelength (>20 km) Bouguer anomaly feature map obtained from low pass filtering analysis of the gravity anomaly map (Figure 9). Anomalies shown on map are primarily related to deep sources. BRUMA - Border Range ultra mafic and mafic assemblages.

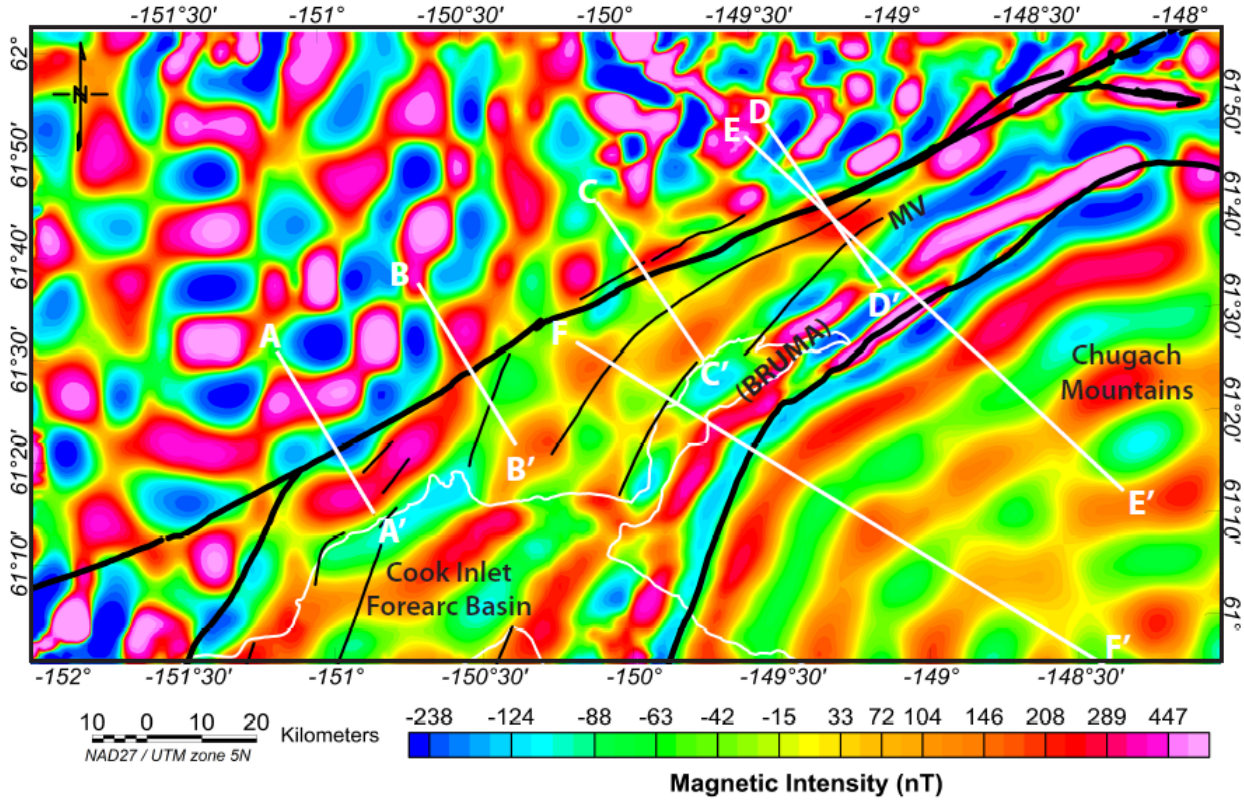

Figure 12. Short-wavelength (<20km) magnetic feature map obtained from high pass filtering analysis of the total intensity aeromagnetic map (Figure 10). These anomalies are primarily related to shallow sources. BRUMA - Border Ranges ultramafic and mafic assemblages. MV - Matanuska Valley.

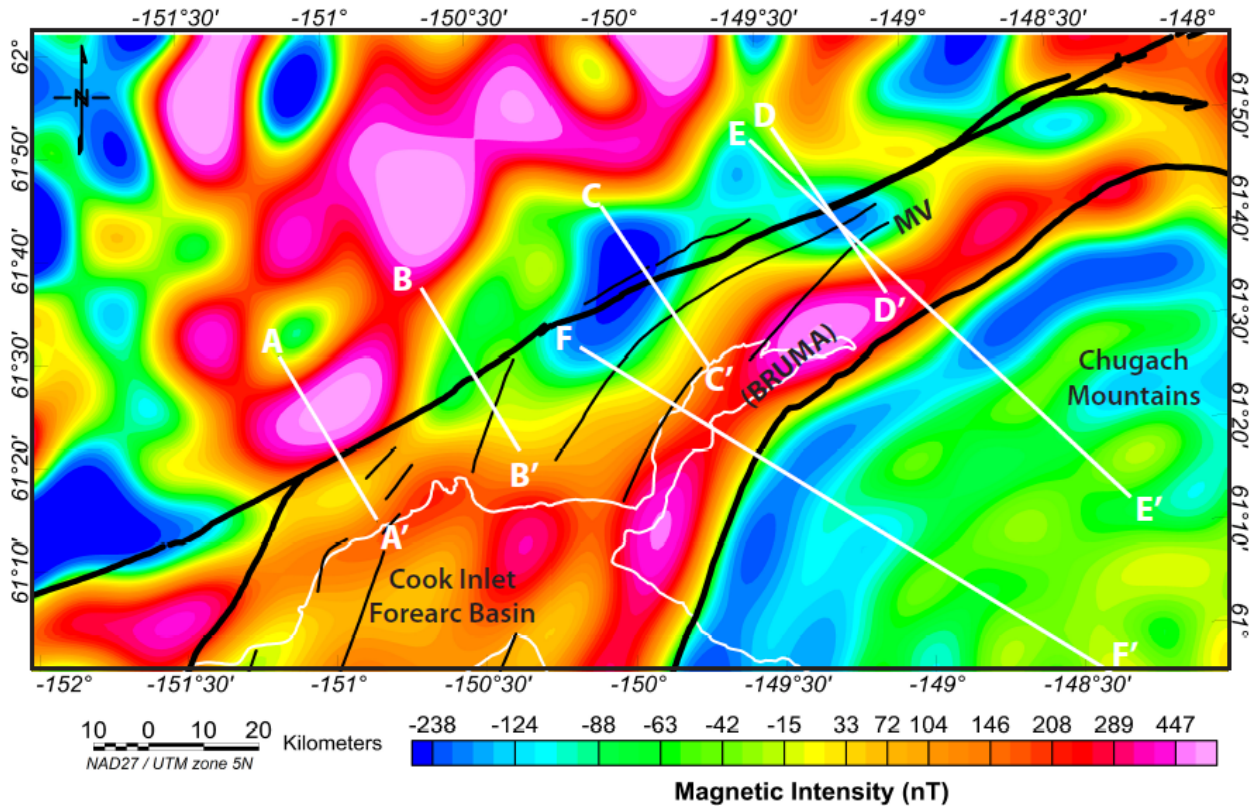

Figure 13. Long-wavelength (>20 km) magnetic feature map obtained from low pass filtering analysis of the total intensity aeromagnetic map (Figure 10). These anomalies are primarily related to deep sources. BRUMA - Border Range ultramafic and mafic assemblages. MV - Matanuska Valley.

DATA CONSTRAINTS FOR 2D FORWARD MODELS

Geosoft GM-SYS modeling software was used to create 2D forward models of the geologic structure across the Castle Mountain Fault. Four parallel transects (profiles A-A', B-B', C-C', and D-D') were selected for the 2D forward modeling shown in Figure 9. All profiles are approximately 32 km in length trending perpendicularly across the CMF in a northwest to southeast direction. Profiles A-A' and B-B' cross the western CMF from the southern Susitna Lowland to the northwestern CIB. Profiles C-C' and D-D' cross the eastern CMF from the southeastern Susitna Lowland/Talkeetna area to the northeastern CIB/Matanuska Valley area. Structures were modeled to a depth of ~50 km and assuming homogeneous bodies extending orthogonal to the profiles to distances of infinity (± 30,000 km).

The modeling software requires reasonable initial estimates of model parameters such as topography, depth, subsurface body shape, density, and magnetization of potential sources. Geologic maps from the U.S. Geological Survey data base compiled by Wilson et al. (2009) were used for geologic contacts and fault constraints. Topographic constraints were applied using digital elevation models from the National Elevation Data set (last updated by Gesch et al., 2002; Gesh, 2007). Geophysical cross-sections from Mankhemthong et al. (2013), Ehm (1983), Shellenbaum et al. (2010), and Li et al. (2013) were used to guide initial depth and thickness estimates for shallow and deep geologic features represented in the 2D models.

Table 1 from Mankhemthong et al. (2013) provides information on subsurface density and magnetic susceptibility variations used in the 2D forward models. Existing profiles E-E' and F-F' created by Mankhemthong et al. (2013) were used as starting models to guide the 2D forward modeling process. All densities and magnetic susceptibilities correspond with Table 1.

Table 1: Densities and Magnetic Susceptibilities used in 2D Forward Modeling

Model bodies	Densities (kg/m^3)	Data sources	Magnetizations (SI)	Data sources
BRUMA	2900–3000	FV, SH	0.030–0.063	A
Basement rocks of Peninsular terrane	2700–2750	FV, EP, SG	0.005†, 0.027*	SH†, Sb*
Granitic intrusions	2500–2700	SH, A	0.010	A
Late Mesozoic rocks	2670–2700	FV	0.005†, 0.027*	A†, SH†, Sb*
Underplated sediments	2550–2600	FV,Y	0.001	A
Early Tertiary sedimentary rocks	2400–2500	DL, SH	0.001	A
Mantle	3300	Sb	0.000	Sb
McHugh Complex of Chugach terrane	2700–2740	HS, NP	0.001–0.006	A, Sa
Accretionary rocks of Prince William terrane	2600–2700	FV	0.002	SG
Serpentinization	2750–2800	FV, SH	0.03–0.13†, 0.04–0.09*	CM†,Sb*
Subducting Pacific plate	2900–3000	Y	0.07–0.09	Sb, SH
Late Tertiary sedimentary rocks	2100–2200	DL, SH	0.001	A, Sa
Valdez Group of Chugach terrane	2690–2720	HS, NP	0.001–0.006	A, Sa
Volcanic arcs	2800	FV, EP	0.025	A
Yakutat microplate	2850	FV	0.017	A

Note: Data source abbreviations: NP—calculated from the Nettleton-Parasnis inversion method (Mankhemthong et al., 2012); FV—converted from seismic tomography data (Fisher and von Huene, 1984); Y—converted from seismic tomography data (Ye et al., 1997); EP—converted from seismic tomography data (Eberhart-Phillips et al., 2006); HS—measured from rock hand samples; DL—determined from density logs; SH—based on Saltus and Haeussler (2004); SG—based on Sanger and Glen (2003); A—based on Altstatt et al. (2002); Sa—based on Saltus et al. (2005); CM—based on Carlson and Miller (2003); Sb—based on Saltus et al. (2007).

Results

Four 2D forward models were created across the Castle Mountain Fault. While models are non-unique, results were produced to exhibit the least structural complexity that honor previous geological and geophysical studies of the region. Three different sedimentary units with varying densities are included in all four models: (1) late Tertiary, (2) early Tertiary, (3) late Mesozoic rock sequences (Table 1); the thicknesses of these units varies across each profile. Approximate thicknesses of these units in the center of CIB are 1800 m, 4000 m, and 4500, respectively. Previous studies report evidence for reverse faulting associated with anticlinal structures throughout the area, however, such features could not be accurately modeled due to the coarse gridding interval (1000 m). These sedimentary units are modeled as overlying the basal crust of the Peninsular terrane basement rocks (Figures 14 and 15). The models increase in geologic complexity from the western to eastern portion of the CMF.

Igneous intrusive plutons (colored red Figure 14) were added along the southwestern portion of the fault to match the higher gravity and magnetic signatures on the northwest side along transects A-A' and B-B'. These features outcrop north of the southwestern segment of the CMF (Figure 2) and are interpreted to be present at depths ranging from 10 to 25 km based on the gravity and magnetic filtering analysis. The sedimentary sequences represented in the models onlap these igneous features within a zone of complex folding along profiles.

Misfits between the observed and calculated magnetic data above the plutons (A-A' and B-B') could be related to the presence of two separately formed plutons. It is possible that these plutons contain similar densities but vary in magnetic susceptibility due to differences in paleomagnetic cooling history. Gravity maps suggest that the pluton associated with A-A' is a fairly self contained, dense intrusion separate from the pluton associated with B-B'. The magnetic maps also suggest that A-A' and B-B' possibly crossed different plutons. A small portion of the magnetic signature for the B-B' pluton could be contributing to the magnetic signal for the A-A' pluton and, while similar in density, could be more highly magnetized.

Profile B-B' shows the best fit between the calculated and observed magnetic anomalies over all the other profiles. Both models (A-A' and B-B') show a good fit between observed and calculated densities related to gravity anomalies along the western CMF.

A serpentinized body was added to constrain broad gravity and magnetic highs along the southeastern segments of C-C' and D-D' (Figure 15). The observed gravity anomalies across profile C-C' match well with anticlinal structures mapped north and south of the fault (Figure 15). However, the magnetic models do not provide a good fit and were estimated significantly higher than the observed magnetic signature. C-C' crosses the CMF over significant long-wavelength gravity and magnetic lows seen on both low pass gravity and magnetic filter maps (Figures 11 and 13). These anomalies are approximately the same length as the 2D models (~34 km) which limit the possibility of accurately modeling deeper long-wavelength causative bodies for the magnetic anomaly data. Short-wavelength anomalies seen on the high pass magnetic filter maps are likely caused by changes in sedimentary thickness across the Matanuska valley (Figure 12). The unfiltered magnetic anomaly map is dominated by long-wavelength magnetic lows trending northeast from the western to eastern segment of the CMF. It is possible that these magnetic lows could be related to a deep structural transition zone corresponding to the southwestern edge of the subducting Yakutat block (Figure 6).

A granitic intrusion was included along the northwestern segment of D-D' to match the gravity high and magnetic low observed over exposed granitic and metamorphic rock units north of the eastern CMF (Figure 15). An ultramafic (BRUMA) block was also added to fit the gravity and magnetic highs adjacent to the ultramafic surface exposures in the northern Chugach Mountain fronts. Misfits between observed and calculated anomalies across the D-D' are reasonable and could be improved with minor adjustments to geometry of subsurface structures and depth to causative bodies. All models fit well with observed gravity data, however, mismatches between observed and calculated magnetic data occurred, particularly along the northwestern parts of profiles A-A' and C-C' in areas that have not been previously modeled.

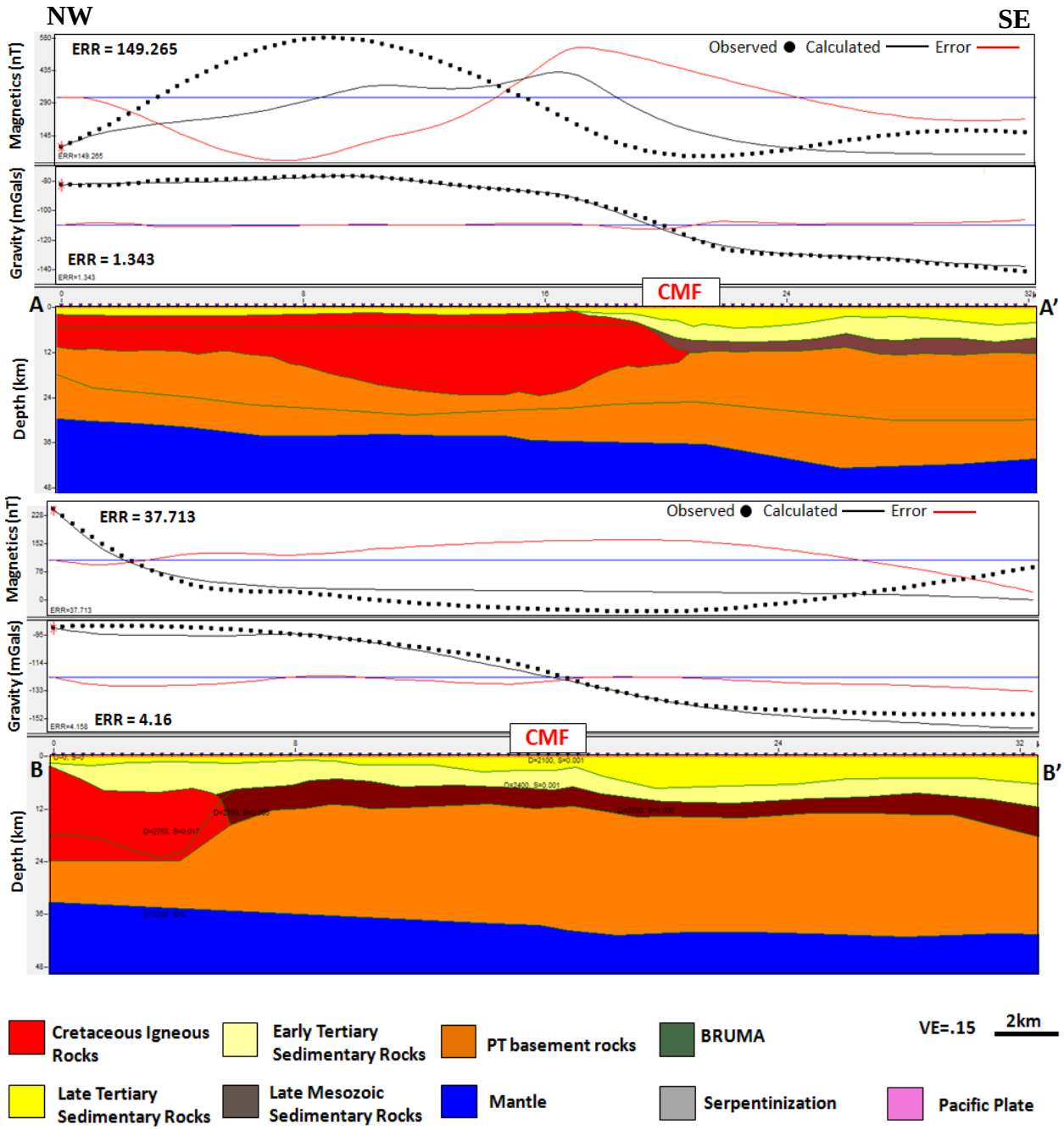

Figure 14. 2D forward gravity and magnetic models arranged from northwest to southeast (A-A', B-B') across the western portion of the Castle Mountain Fault. Density and magnetic constraints are given in Table 1. CMF indicated in red above each profile is the location of the Castle Mountain Fault.

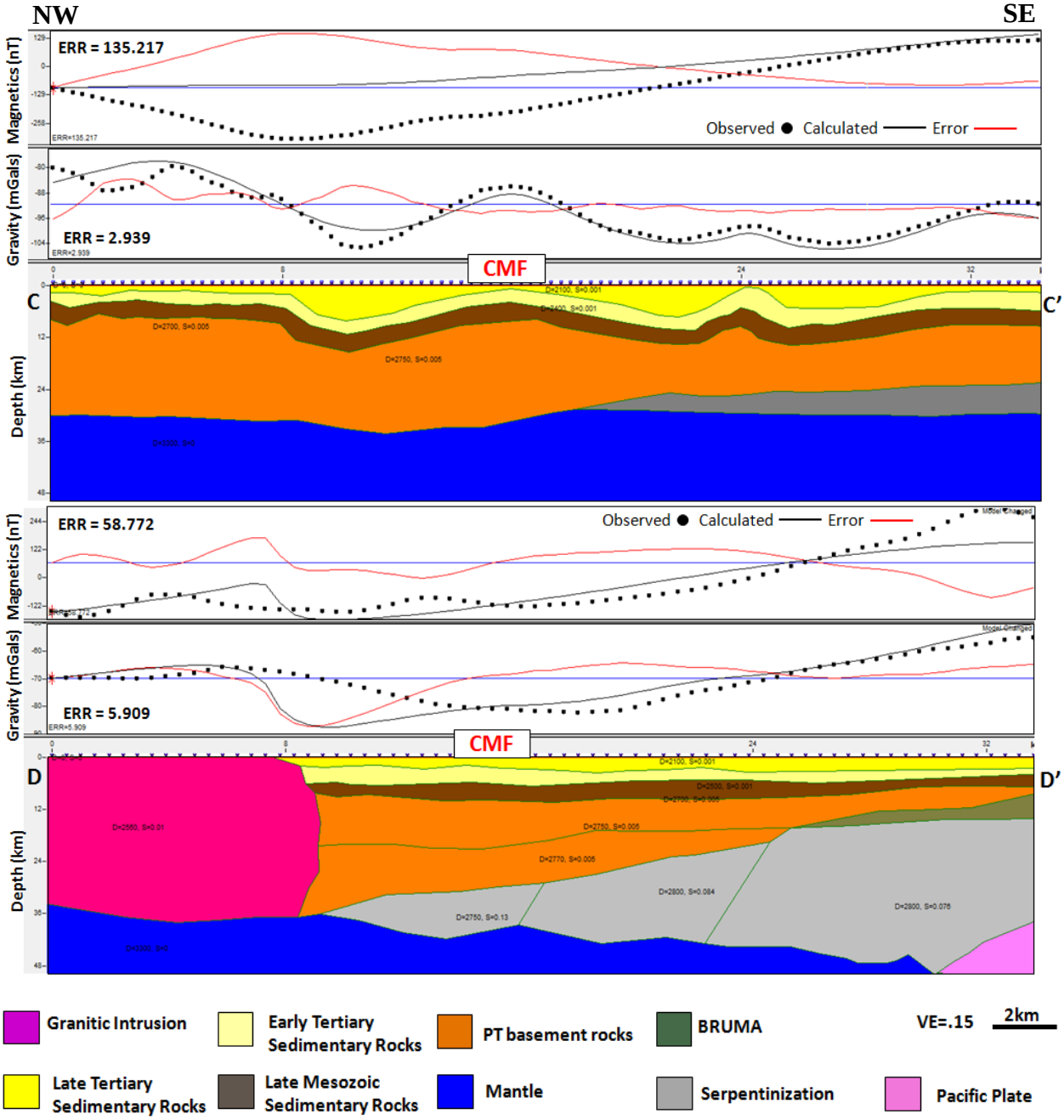

Figure 15. 2D forward gravity and magnetic models arranged from northwest to southeast (C-C', D-D') across the eastern portion of the Castle Mountain Fault. Density and magnetic constraints are given in Table 1. CMF indicated in red above each profile is the location of the Castle Mountain Fault.

Conclusions

Four detailed 2D forward models were created across the Castle Mountain Fault using newly collected gravity data with constraints from existing aeromagnetic data and previous geological and geophysical studies. Short-wave length high pass and long-wavelength low-pass filter maps were incorporated into the modeling process to emphasize shallow and deep crustal structures within the 2D models. These integrated models help to characterize crustal differences between the western and eastern portions of the Castle Mountain Fault.

The granitic intrusion modeled in A-A' occurs along the southwestern portion of the CMF within close proximity to the Bruin Bay fault splay which borders the northwestern margin of the CIB. A-A' suggests this intrusion could influence the fault splay forming the western edge of the CIB. B-B' and C-C' are closest to the area consisting of mapped fault scarps, however, these profiles intersect the CMF where we see very little contrast within 5-10 km of the sedimentary section on either side of the fault. A strong transition occurs between B-B' and C-C' between paleoseismically active to recently active seismicity with no surface expression. This transition crosses the edge of the Yakutat block. Low-pass filter maps show evidence for deeper structures within this zone. Relocated seismicity maps show minimal seismicity between these profiles. Seismicity increases along the northeastern segment of the CMF within close proximity to D-D'. A large granitic intrusion along the northwestern side of D-D' is modeled within 5 km of the fault. This granitic intrusion most likely has some effect on the mechanical behavior of the fault where sediments are being pinched out and serpentinization is occurring. The bedrock structure of the eastern portion of the fault contains dense serpentinized features not present in the western segments. Historic and recent seismicity occurring south of the CMF could be related to serpentinization in Cook Inlet which cuts off at the end of the CIB. Seismicity north of the CMF is concentrated within gravity highs.

All models fit well with observed gravity data, however, mismatches between observed and calculated magnetic data occurred, particularly along the northwestern parts of profiles A-A'

and C-C'. Our profiles were constructed over challenging areas that have not been previously modeled. Continued modeling could examine the possibility of two igneous intrusions of different paleomagnetic cooling ages beneath the Susitna Lowland basin. Incorporating two separate plutons with similar densities but different compositional magnetization could result in a better match between the observed and calculated magnetic anomaly data over the western segment of the CMF. Continued modeling could also examine the deeper magnetic and gravity lows across C-C'. Our inability to accurately model these anomalies could be related to the fact that the longer-wavelength feature could require a much longer regional profile to adequately see the effects of the structure observed in strong gravity and magnetic lows. Fluctuations in sedimentary thickness also complicate modeling the effects of deeper structures across the fault and could be addressed by constructing a regional model.

References

Alaska Earthquake Information Center, 2014, AEIC earthquake database search: http://www.aeic.alaska.edu/html_docs/db2catalog.html (accessed January 2014).

Blakey, R.J., 1995, Potential theory in gravity and magnetic applications: Cambridge, UK, Cambridge University Press, 136 p.

Burger, R.H., Sheehan, A.F., and Jones, C.H., 2006, Introduction to applied geophysics: Exploring the shallow subsurface: New York, W.W. Norton, 554 p.

Brocher, T.M., G.S. Fuis, M.A. Fisher, G. Plafker, M.J. Moses, J.J. Taber, and N.I. Christensen, 1994, Mapping the megathrust beneath the northern Gulf of Alaska using wide-angle seismic data, J. Geophys. Res. 99, 663-686.

Cardenas, R., M. Ceberio, 2012, Efficient geophysical technique of vertical line elements as a natural consequence of general constraints techniques, J. Uncert. Syst. 6, 86-88.

Doser, D.I., N.A. Ratchkovski, P.J. Haeussler, and R. Saltus, 2004, Changes in crustal seismic deformation rates associated with the 1964 Great Alaska earthquake: Bull. Seismol. Soc. Amer. 94, 320-325.

Debari, S.M., and Coleman, R.G., Exhumation of the deep levels of an island arc, the Tonsina ultramafic assemblage, Tonsina, Alaska: Journal of Geophysical Research, v. 94, p.4373-4391, doi:10.1029/JB094iB04p04373.

Detterman, R.L., Plafker, G., Tysdal, R.G., and Pavoni, N., 1974, Surface geology and Holocene breaks along the Susitna segment of the Castle Mountain fault, Alaska: U.S. Geological Survey Miscellaneous Field Studies Map MF-618, 1 plate, scale 1:24,000.

Ehm, A., 1983, Oil and gas basins map of Alaska: Alaska Division of Geological and Geophysical Surveys Special Report 32, 1 sheet, scale 1:2,500,000

Flores, C. and D. I. Doser, 2005, Shallow seismicity of the Anchorage, Alaska region: Bull. Seismol. Soc. Am.,95, 1865-1879.

GEsch, D.B., Oimoen, M., Greenlee, S., Nelson, C., Steuck, M., and Tyler, D., 2002 The National Elevation Dataset: Photogrammetric Engineering and Remote Sensing, v. 68, p. 5-11.

Gesch, D.B., 2007, The National Elevation Dataset, *in* Maune, D., ed., Digital elevation model technologies and applications: The DEM users manual (second edition): Bethesda, Maryland, American Society for Photogrammetry and Remote Sensing, p.99-118.

Haeussler, P. J., 1994, Possible active fault traces on or near the Castle Mountain fault between Houston and the Hatcher Pass Road: in Till, A., and T. Moore, eds., Geologic studies in Alaska by the U.S. Geol.Surv. 1993, U.S. Geol. Surv. Bull. 2107, 49-58.

Haeussler, P., and R. Saltus, 2011, Location and extent of Tertiary structures in Cook Inlet Basin, Alaska, and mantle dynamics that focus deformation and subsidence, Prof. Paper 1776-D.

Haeussler, P., R. L. Bruhn, and T.L. Pratt, 2000, Potential seismic hazards and tectonics of Upper Cook Inlet Basin, Alaska, based on Pliocene and younger deformation: Geol. Soc. Am. Bull. 112, 1414-1429.

Haeussler, P.J., T.C. Best and C.F. Waythomas, 2002, Paleoseismology at high latitudes: Seismic disturbance of upper Quaternary deposits along the Castle Mountain fault near Houston, Alaska: Geol. Soc. Am. Bull. 114, 1296-1310.

Lahr, J.C., R.A. Page, C.D. Stephens and K.A. Fogleman, 1986, Sutton, Alaska, earthquake of 1984: evidence for activity on the Talkeetna segment of the Castle Mountain fault system: Bull. Seism. Soc. Am. 76, 967-983.

Mankhemthong, N., Doser, D.I., and Baker, M.R., 2012, Practical estimation of near surface bulk density variations across the Border Ranges fault system, central Kenai Peninsula, Alaska, Journal of Environmental & Engineering Geophysics, v. 17, p. 151-158, doi:10.2113/JEEG17.3.151.

Mankhemthong, N., D.I. Doser, M.R. Baker and R. Cardenas, Constraints on the structure of the Border Ranges fault system, south-central Alaska, from the integrated 3-D inversion of gravity data, Geol. Soc. Amer. Rocky Mtn. Section Meeting, Albuquerque, NM, abstract 34-10, May 2012b.

Mankhemthong, N., Doser, D.I., and Pavlis, T.L., 2013, Interpretations of gravity and magnetic data and development of 2.5D cross sectional models for the Border Ranges fault system, south-central Alaska, Geoshpere, v. 9, p. 242-259, doi:10.1130/GES00833.1.

Merritt, R.D., 1986 Paleoenvironmental and tectonic controls in major coal basins of Alaska, *in* Lyons, P.C., and Rice, C.L., eds., Paleoenvironmental and Tectonic Controals in Coal-Forming Basins in the United States: Geological Society of America Special Paper 210, p. 173-200.

Meyer, J.F. and Boggess, P.L., 2003, Principal facts for gravity data collected in the Susitna area, southcentral Alaska: Alaska Division of Geological & Geophysical Surveys Preliminary Interpretive Report 2003-3, 13 p.

Nokleberg, W.J., Plafker, G. & Wilson, F.H., 1994, Geology of south-central Alaska, *in* Plafker, G., and Berg, H.C., eds., The Geology of Alaska; Boulder, Colorado, Geological Society of America, Geology of North America, v. G-1, p. 311-366.

Pavlis, T.L., and Roeske, S.M., 2007, The Border Ranges fault system, southern Alaska, *in* Ridgway, K.D., et al., eds., Tectonic growth of a collisional continental margin: Crustal evolution of southern Alaska: Geological Society of America Special Paper 431, p. 95-128, doi:10.1130/2007.2431(05).

Plafker, G., Nokleberg, W., and Lull, J., 1989 Bedrock geology and tectonic evolution of the Wrangellia Peninsular, and Chugach terranes along the Trans-Alaska Crustal Transect in the Chugach Mountains and southern Copper River Basin, Alaska: Journal of Geophysical Research, v. 94, p. 4255-4295, doi:10.1029/JB094iB04p04255.

Ratchkovski, N.A., R.A. Hansen, J.C. Stachnik, T. Cox, O. Fox, L. Rao, E. Clark, M. Lafevers, S. Estes, J.B. MacCormack, and T. Williams, 2003, Aftershock sequence of the Mw 7.9 Denali fault, Alaska, earthquake of 3 November 2002 from regional seismic network data: Seismol. Res. Lett., 74, 743-752.

Saltus, R.W., G.G. Connard and P.L. Hill, 1999, Alaska Aeromagnetic Compilation-Digital Grids and Survey Data, U.S. Geol. Surv. Open File Rept. 99-502.

Saltus, R.W., P.J. Haeussler, R.E. Bracken, J.P. Doucette, and R.C. Jachens, 2001, Anchorage urban region aeromagnetics (AURA) project: preliminary geophysical results, U.S. Geol. Surv. Open-File Rept. OF 01-0085, 21 pp.

Saltus, R.W., and Simmons, G.C., 1997, Composite and merged aeromagnetic data for Alaska: A website for distribution of gridded data and plot files: U.S. Geol. Surv. Open-file Rept. 97-520, http://geology.cr.usgs.gov/pub/open-file-reports/ofr-97-0520/.

Saltus, R.W., Hudson, T.L., and Wilson, F.H., 2007, The geophysical character of southern Alaska-Implications for crustal evolution *in* Ridgway, K.D., et al., eds., Tectonic growth of a collisional continental margin: Crustal evolution of Southern Alaska: Geological Society of America Special Paper 431, p. 1-20, doi:10.113/2007.2431(01).

Sanger, E.A., and Glen, J.M.G., 2003, Density and magnetic susceptibility values for rocks in the Talkeetna Mountains and adjacent region, south-central Alaska: U.S. Geological Survey Open-File Report 03-268, 42 p.

Shellenbaum, D.P., Gregersen, L.J., and Delaney, P.R., 2010, Top Mesozoic unconformity depth map of the Cook Inlet basin, Alaska: Alaska Division of Geological and Geophysical Surveys Report of Investigation 2010-2, 1 sheet, scale 1:500,000.

Swenson, R.F., 1997, Introduction to Tertiary tectonics and sedimentation in the Cook Inlet Basin, *in* Karl, S. M., Vaughn, N.R., and Ryherd, T.J., eds., 1997 Guide to the geolog of the Kenai Peninsula, Alaska: Geological Society, p. 18-27.

Trop, J.M., Szuch, D.A., Rioux, M., and Blodgett, R.B., 2005, Sedimentology and provenance of the Upper Jurassic Naknek Formation, Talkeetna Mountains, Alaska: Bearings on the accretionary tectonic history of the Wrangellia composite terrane: Geological Society of America Bulletin, v. 117, p. 570-588, doi:10.113/B25575.1.

Tysdal, R.G., Plafker, G., 1978, Age and continuity of the Valdez Group, southern Alaska, *in* Sohl, N.F., and Wright, W.B., eds., Changes in stratigraphic nomenclature by the U.S. Geological Survey, 1977: U.S. Geological Survey Bulletin 1457-A, p. A120-A124.

Wesson, R.L., A.D. Frankel, C.S. Mueller, and S.C. Harmsen, 1999, Probabilistic seismic hazard maps of Alaska: U.S. Geol. Surv. Open File Rept. 99-36, 20 pp.

Willis, J.B., P.J. Haeussler, R.L. Bruhn, and G.C. Willis, 2007, Holocene slip rate for the western segment of the Castle Mountain fault: Alaska, Bull. Seism. Soc. Am. 97, 1019-1024.

Wilson, F.H., Hults, C.P., Schmoll, H.R., Haeussler, P.J., Schmidt, H.M., Yehle, L.A., and Labay, K.A., 2009, Preliminary geologic map of the Cook Inlet region, Alaska: U.S. Geological Survey Open-file Report 2009-1108, http://pubs.usgs.gov/of/2009/1108/.

Vita

Shane Schinagel was born in El Paso, TX on September 6, 1984. He began studying Geology in the fall of 2009 at El Paso Community College while working full-time as an escrow assistant at Sierra Title Company. In the fall of 2010 he quit his job in the title industry to enroll full-time in the B.S. Geophysics program at the University of Texas - El Paso (UTEP). As an undergraduate student he began conducting active geophysical research focusing on seismicity and tectonics of south-central Alaska under the guidance of Dr. Diane Doser.

During the spring semester of 2012 Shane received several scholarships, honors, and awards recognizing excellence for outstanding research in geophysics. The HSF and Marathon Oil awarded him a $30,000 scholarship as an undergraduate which also included a paid summer internship as a geophysicist with Marathon Oil in Houston, TX. Upon completing his first internship, Marathon Oil extended him a return internship offer for the summer of 2013 in addition to nominating him into the National GEM Fellowship which would pay for his graduate education in full. After receiving his B.S.-Geophysics he immediately enrolled into the M.S.-Geophysics program at UTEP and continued to work with Dr. Diane Doser.

As a graduate student he completed two more internships with Marathon Oil over the summers of 2013 and 2014 before receiving a full-time job offer. Between summer internships he served as a student representative for Marathon oil promoting petroleum oriented opportunities within the geosciences made available by Marathon Oil. He also fulfilled all responsibilities associated with several undergraduate and graduate level teaching assignments including Geology for Civil Engineers, and Geophysical Well Logging. He was awarded his M.S. in Geophysics in May 2015 and began working as a full-time geophysicist for Marathon Oil over the summer of 2015.

Permanent address: 8520 Morley Dr.

El Paso, TX 79925

This thesis/dissertation was typed by Shane Schinagel.